
Online Binary Space Partitioning Forests

Xuhui Fan

School of Mathematics and Statistics
University of New South Wales
xuhui.fan@unsw.edu.au

Bin Li

School of Computer Science
Fudan University
libin@fudan.edu.cn

Scott A. Sisson

School of Mathematics and Statistics
University of New South Wales
scott.sisson@unsw.edu.au

Abstract

The Binary Space Partitioning-Tree (BSP-Tree) process was recently proposed as an efficient strategy for space partitioning tasks. Because it uses more than one dimension to partition the space, the BSP-Tree Process is more efficient and flexible than conventional axis-aligned cutting strategies. However, due to its batch learning setting, it is not well suited to large-scale classification and regression problems. In this paper, we develop an online BSP-Forest framework to address this limitation. With the arrival of new data, the resulting online algorithm can simultaneously expand the space coverage and refine the partition structure, with guaranteed universal consistency for both classification and regression problems. The effectiveness and competitive performance of the online BSP-Forest is verified via simulations on real-world datasets.

1 Introduction

The BSP-Tree Process [Fan et al., 2016a, Fan et al., 2018a, Fan et al., 2019b] is a stochastic space partitioning process defined in a multi-dimensional space with a binary-partition strategy. Its general goal is to identify meaningful “blocks” in the space, so that data within each block exhibits some form of homogeneity. Similar to other space partitioning processes [Kemp et al., 2006, Roy and Teh, 2009, Nakano et al., 2014, Fan et al., 2018b], the BSP-Tree Process can be applied in many areas, including relational modeling [Kemp et al., 2006, Airolidi et al., 2009, Fan et al., 2016b, Fan et al., 2019a], community detection [Nowicki and Snijders, 2001, Karrer and Newman, 2011], collaborative filter-

ing [Porteous et al., 2008, Li et al., 2009], and random forests [Lakshminarayanan et al., 2014].

Instead of the axis-aligned cuts adopted in most conventional approaches [Kemp et al., 2006, Roy and Teh, 2009, Nakano et al., 2014], the BSP-Tree Process implements oblique cuts (in more than one dimension) to recursively partition the space into new sub-spaces. In this way, it can describe the dimensional dependence more efficiently, in terms of fewer cuts or improved prediction performance. In addition, the BSP-Tree Process has the attractive theoretical property of self-consistency. Based on this property, a projective system [Crane, 2012] can be constructed to ensure distributional invariance, when restricting the process from a larger domain to a smaller one, and safely extend a finite domain to multi-dimensional infinite space.

Despite the existing clear potentials, there are two main challenges in the BSP-Tree Process. (1) *Scalability*: Its batch learning mode is unappealing given the practical real, large-scale datasets, as multiple scans over the data are required. (2) *Theoretical properties*: Moving from a batch to an online learning algorithm, rigorous universal consistency properties are required to ensure the theoretical correctness of the underlying BSP-Tree Process prior as the domain varies with the arrival of new data. This can be challenging due to the recursive structure of the partition strategy and the Markov property of partition refinement.

In this paper we propose an online BSP-Forest framework to address these challenges. Instead of batch model training, our framework sequentially incorporates each data point and updates the model without the need for data labels. The tree structure update in the forest is implemented in two stages. (i) *Node coverage expansion*: Within the nodes (all of nodes are convex polyhedron-shaped) of each tree, we focus on the convex hull that contains all of its allocated datapoints. When a new point arrives in this node but falls outside the convex hull, we enlarge the hull and change the tree structure. (ii) *Refinement over existing partitions*: We use a monotonically increasing budget sequence for new node creation, meaning that more data tend to result in finer partitions. These stages are each supported by the self-consistency and Markov properties of the BSP-Tree

Process. In addition, we demonstrate its universal consistency by proving that the online BSP-Forest will converge to the Bayesian error for all possible label distributions. The effectiveness and competitive performance of the online BSP-Forest in classification and regression is verified through extensive simulation studies.

2 The BSP-Tree Process

The BSP-Tree Process [Fan et al., 2018a, Fan et al., 2019b] is a time-indexed, right-continuous Markov jump process. At any point of the time line, the BSP-Tree Process takes the state of a hierarchical binary partition over the multi-dimensional space (Figure 1). Starting at time 0 with the initial space (no cuts), new random oblique cuts are created over time. Each selected region for partition is named a block, where each cut recursively divides the block into two smaller ones. Given any two time points $0 < t_1 \leq t_2$, the partition at t_2 is a further refinement of the partition at t_1 (e.g. there might be additional cuts).

The distinguishing feature of the BSP-Tree Process is the oblique cut it uses to partition the space. Unlike its axis-aligned cut counterparts [Roy and Teh, 2009], the BSP-Tree Process uses more than one dimension to form the cutting hyperplanes, and so is a more efficient cutting strategy (i.e. it uses fewer cuts to achieve similar performance).

We introduce some notation before formally describing the BSP-Tree Process. For a d -dimensional space \square (which is assumed to be a convex polyhedron), we let $\mathcal{D} = \{(1, 2), (1, 3), \dots, (d-1, d)\}$ denote the set of all two dimensional pairs. For each element (d_1, d_2) in \mathcal{D} , $\Pi_{d_1, d_2}(\square)$ denotes the projection of \square onto the dimensions of (d_1, d_2) (which becomes a 2-dimensional polygon), $L_{(d_1, d_2)}(\square)$ denotes the corresponding perimeter, $\mathbf{l}_{\Pi_{d_1, d_2}(\square)}(\theta)$ lies in the 2D space of dimensions (d_1, d_2) and represents the line segment of $\Pi_{d_1, d_2}(\square)$ in the direction of the angle θ (in the dimensions of (d_1, d_2) ; Figure 1 (Right)), \mathbf{u} is the cutting position in the segment $\mathbf{l}_{\Pi_{d_1, d_2}(\square)}(\theta)$, c represents the cost of a cut in the time line and $C = (c, (d_1^*, d_2^*), \theta, \mathbf{u})$ represents one cutting hyperplane with all these variables.

Algorithm 1 describes generation of the recursive hierarchical partition under the BSP-Tree Process. Algorithm 2 generates an oblique cut in a particular block \square ; the right part of Figure 1 illustrates Lines 3–6 in Algorithm 2. To generate an oblique cut in \square , we first generate the cost of the proposed cut from an Exponential distribution, parameterised by the sum of perimeters of all of the block’s two-dimensional projections (Line 1). If $c > \tau$ so the cost of the candidate cut exceeds the budget τ , the cut is not generated and the current block \square is returned as the final partition structure in that branch (Line 9); otherwise we sample a 2-dimensional pair (d_1^*, d_2^*) in proportion to $\{L_{(d_1, d_2)}(\square)\}_{(d_1, d_2) \in \mathcal{D}}$ (Line 3). The cutting hyperplane will be generated in this dimensional pair, and is parallel

Algorithm 1 BSP (\square, τ)

1: Call BlockCut(\square, τ)

Algorithm 2 BlockCut (\square, τ)

1: Sample cost $c \sim \text{Exp}(\sum_{(d_1, d_2) \in \mathcal{D}} L_{(d_1, d_2)}(\square))$

2: **if** $c < \tau$ **then**

3: $(d_1^*, d_2^*) \sim p(d_1, d_2) \propto L_{(d_1, d_2)}(\square), (d_1, d_2) \in \mathcal{D}$

4: $\theta^* \sim p(\theta) \propto |\mathbf{l}_{\Pi_{d_1^*, d_2^*}(\square)}(\theta)|, \theta \in (0, \pi]$, Sample \mathbf{u} uniformly on $\mathbf{l}_{\Pi_{d_1^*, d_2^*}(\square)}(\theta^*)$

5: Form cutting hyperplane $H((d_1^*, d_2^*), \theta^*, \mathbf{u})$ and cut \square into two sub-blocks \square', \square''

6: $\mathcal{B}' = \text{BlockCut}(\square', \tau - c)$, $\mathcal{B}'' = \text{BlockCut}(\square'', \tau - c)$

7: Return $\{\square, C = \{c, (d_1^*, d_2^*), \theta^*, \mathbf{u}\}, \mathcal{B}', \mathcal{B}''\}$

8: **else**

9: Return $\{\square, \emptyset, \emptyset, \emptyset\}$

10: **end if**

to the other dimensions. Line 4 generates the angle θ^* with density proportional to $|\mathbf{l}_{\Pi_{d_1^*, d_2^*}(\square)}(\theta)|$, and the cutting position \mathbf{u} uniformly in the segment $\mathbf{l}_{\Pi_{d_1^*, d_2^*}(\square)}(\theta^*)$ for the pair (d_1^*, d_2^*) . The cutting hyperplane is then formed as $H((d_1^*, d_2^*), \theta^*, \mathbf{u}) = \{\mathbf{x} \in \square \mid [(x_{d_1^*}, x_{d_2^*}) - \mathbf{u}](1; \tan \theta^*)^\top = 0\}$ and cuts the block \square into two new sub-blocks (Line 5). Line 6 recursively generates *independent* BSP partitions $\mathcal{B}', \mathcal{B}''$ on the new blocks \square', \square'' .

One attractive property of BSP-Tree Process is that it is self-consistent [Fan et al., 2018a, Fan et al., 2019b]. This helps to provide an efficient convex hull representation of nodes in a tree when in a multi-dimensional space.

Theorem 1. (Self-Consistency) *Given a partition sampled from the BSP-Tree Process on the convex domain \square , let $\Delta \subset \square$ be a convex subdomain of \square . Then, the restriction of this partition on Δ has the same distribution as the restriction directly sampled from the BSP-Tree Process on Δ .*

3 Online BSP-Forests

We have an observed set of N labelled datapoints $\{(\mathbf{x}_n, y_n)\}_{n=1}^N \in \mathbb{R}^d \times \mathbb{R}$ which arrive over time, where \mathbf{x}_i is a d -dimensional feature vector and y_i is the corresponding label. We have an additional set of feature data for predictive testing. The goal is to predict the unknown labels of the testing data, based on their feature data and the observed training data $\{(\mathbf{x}_n, y_n)\}_{n=1}^N$.

Similar to the standard random forest [Breiman, 2000, Biau et al., 2008], which assumes the partition is generated independently of the data labels, the online BSP-Forest does not use the data labels, but considers the partition structure within the convex hulls spanned by the arrival feature data \mathbf{x} . Each node in the BSP-Tree records two items: the convex hull that covers its constituent datapoints, and the possible hyperplane cutting this hull. A nested set $\mathcal{V}^{(0)}$ may be used to represent the tree struc-

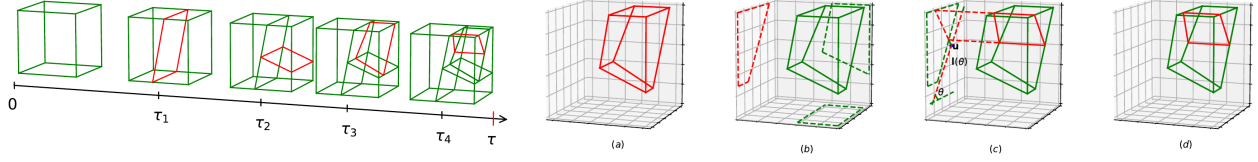


Figure 1: Left: a realisation of a 3-dimensional BSP-Tree Process with budget τ . Each red-line constituted polygon denotes a new cutting hyperplane generated at a particular time. Right: visualization of generating a cutting hyperplane in a 3-dimensional block \square in Algorithm 2: (a) Visualize the block \square ; (b) Select the dimensional pair; (c) Sample the direction θ and cut position \mathbf{u} ; and (d) Form a new cut in \square .

Algorithm 3 oBSP($\mathbf{x}_{1:N}, \tau_{1:N}$)

- 1: Initialise $\mathcal{V}^{(0)}(m) = \{\emptyset, \emptyset, \emptyset\}, \forall m \in \{1, \dots, M\}$
 - 2: **for** $n = 1, \dots, N$ **do**
 - 3: $\mathcal{V}^{(0)}(m) = \text{cBSP}(\mathcal{V}^{(0)}(m), \mathbf{x}_n, \tau_n), \forall m \in \{1, \dots, M\}$
 - 4: **end for**
-

ture of these nodes. $\forall l \in \{0, \dots, L\}$, $\mathcal{V}^{(l)}$ is defined as $\mathcal{V}^{(l)} = \{\diamond^{(l)}, C^{(l)}, \mathcal{V}_{\text{left}}^{(l+1)}, \mathcal{V}_{\text{right}}^{(l+1)}\}$, where $\diamond^{(l)}$ refers to the given convex hull, $C^{(l)}$ is $\diamond^{(l)}$'s cutting hyperplane, and $\mathcal{V}_{\text{left}}^{(l+1)}$ ($\mathcal{V}_{\text{right}}^{(l+1)}$) represents the left (right) child node of $\mathcal{V}^{(l)}$. Since $\mathcal{V}^{(0)}$ is generated depending on the feature points $\mathbf{x}_{1:N}$, it can be generated as $\mathcal{V}^{(0)} \sim \text{BSP}_{\mathbf{x}}(\mathbf{x}_{1:N}, \tau_{1:N})$, where $\tau_{1:N}$ is an increasing budget sequence.

Further, the BSP-Forest, an ensemble of M independent BSP-Trees $\{\mathcal{V}^{(0)}(m)\}_{m=1}^M$ sampled over the feature space, may be used for regression/classification tasks. In this way, the predictive label distribution on any feature data \mathbf{x}_n is $g(\mathbf{x}_n) = \frac{1}{M} \sum_{m=1}^M p(y|\mathbf{x}_n, \mathcal{V}^{(0)}(m))$, where $p(y|\mathbf{x}_n, \mathcal{V}^{(0)}(m))$ is the predictive distribution of y under the m -th BSP-Tree. That is, the predictive distribution is a finite sample approximation to $\mathbb{E}_{\mathcal{V}^{(0)} \sim \text{BSP}_{\mathbf{x}}(\mathbf{x}_{1:N}, \tau_{1:N})} [p(y|\mathbf{x}, \mathcal{V}^{(0)})]$, which becomes more accurate for a larger M .

Algorithm 3 (oBSP, along with Algorithms 4 and 6) specifies the strategy of building the online BSP-Forest in detail. Starting from a set of empty nodes, the online BSP-Forest updates each BSP-Tree once new training data \mathbf{x}_{n+1} arrives. From the BSP-Tree constructed from the previous n datapoints, this procedure then defines a *conditional* BSP-Tree Process (cBSP) such that, following the distributional invariance self-consistency property between the domain and its subdomain, and the Markov property in the time line, the new partition $\mathcal{V}'^{(0)}$ based on up to $n+1$ datapoints is constructed as

$$\mathcal{V}^{(0)} \sim \text{BSP}_{\mathbf{x}}(\mathbf{x}_{1:n}, \tau_{1:n}), \mathcal{V}'^{(0)} \sim \text{cBSP}(\mathcal{V}^{(0)}, \mathbf{x}_{n+1}, \tau_{n+1}).$$

It then follows that the new partition $\mathcal{V}'^{(0)}$ has the same distribution as

$$\mathcal{V}'^{(0)} \sim \text{BSP}_{\mathbf{x}}(\mathbf{x}_{1:n+1}, \tau_{1:n+1}).$$

That is, the distribution of an online BSP-Tree trained (using

Algorithm 4 cBSP($\mathcal{V}^{(l)} = \{\diamond^{(l)}, C^{(l)}, \mathcal{V}_{\text{left}}^{(l+1)}, \mathcal{V}_{\text{right}}^{(l+1)}\}, \mathbf{x}, \tau$)

- 1: Define \diamond' as convex hull covering both $\diamond^{(l)}$ and \mathbf{x} .
 - 2: **if** \diamond' contains ≤ 3 datapoints **then**
 - 3: Replace $\diamond^{(l)}$ with \diamond' in $\mathcal{V}^{(l)}$ and return $\mathcal{V}^{(l)}$
 - 4: **else if** $\mathcal{V}^{(l)}$ is a leaf node **then**
 - 5: Return HullCut($\diamond^{(l)}, \tau$) // $\diamond^{(l)}$ is the convex hull in $\mathcal{V}^{(l)}$
 - 6: **end if**
 - 7: Sample a cost variable $c' \sim \text{Exp}(\lambda)$, where $\lambda = \sum_{(d_1, d_2) \in \mathcal{D}} [L_{(d_1, d_2)}(\diamond') - L_{(d_1, d_2)}(\diamond^{(l)})]$
 - 8: **if** $c' < c^{(l)}$ **then** // $c^{(l)}$ is the cut cost in $C^{(l)}$
 - 9: Generate cut C' in \diamond' , with C' not crossing into $\diamond^{(l)}$
 - 10: Increase all the level index (l) in $\mathcal{V}^{(l)}$ by 1, return $\mathcal{V}^{(l)} = \{\diamond', C', \mathcal{V}^{(l+1)}, \{\mathbf{x}, \emptyset, \emptyset\}\}$
 - 11: **else**
 - 12: **if** $\mathbf{x} \notin \diamond^{(l)}$ **then**
 - 13: Extend current cut $C^{(l)}$ to \diamond' and use \diamond' to replace $\diamond^{(l)}$
 - 14: **end if**
 - 15: cBSP($\mathcal{V}_{\text{left}}^{(l)}, \mathbf{x}, \tau - c^{(l)}$) // assume that \mathbf{x} belongs to the left side of $C^{(l)}$
 - 16: **end if**
-

the cBSP) on sequentially arriving data, is the same as that of a BSP-Tree (BSP $_{\mathbf{x}}$) directly trained on the full dataset. Different shuffling arrangement on the datapoints would not affect the partition result.

Conditional BSP-Tree Process (cBSP): Algorithm 4 describes the procedural detail of the cBSP when incorporating a new datapoint \mathbf{x} . Based on the location of \mathbf{x} and the (possibly) generated cut cost, each BSP-Tree might update the tree structure, enlarge the hull coverage, or implement a new cut in the tree nodes. Figure 2 illustrates each of these cases:

- (i) Points a, b, c, d form a 2-level BSP-Tree (Lines 1–6, Algorithm 4), where a, b, c are in the right level-1 convex hull and d is in the left one.
- (ii) A new point e arrives outside the level-0 convex hull. A new cost value c' is generated (Line 7, Algorithm 4). This new cost c' is compared with the cost c associated with the cut-line in the level-0 convex hull. If $c' < c$ (Line 8, Algorithm 4), a cut-line not crossing into the level-0 convex hull is generated (see Section 1 of the supplementary material), and a new level-0 convex hull is formed from the previous level-0 hull and the point

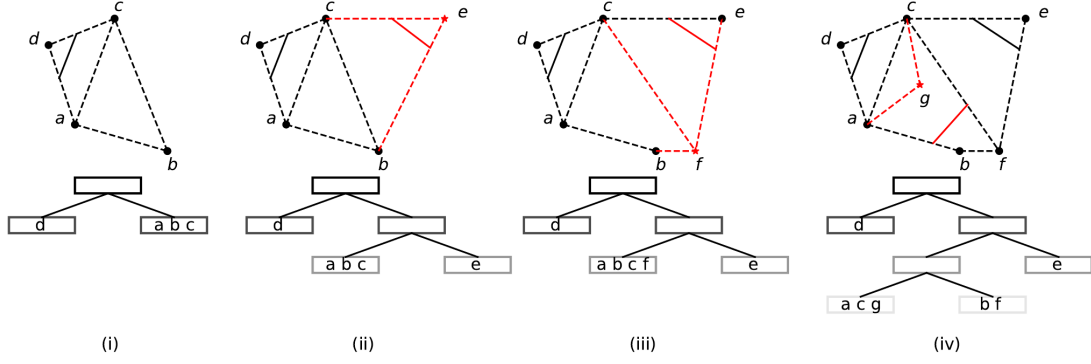


Figure 2: Steps (i)–(iv): A 2-dimensional illustration of a sequence of online BSP-Tree updates on arrival of new datapoints (denoted by \star). Dashed lines indicate edges of convex hulls and solid lines represent cutting lines. Black and red colouring respectively denotes existing and newly active components at the current step. The tree structure (bottom figure) can be identified through the subset relations between the convex hulls.

Algorithm 5 HullCut (\diamond, τ)

- 1: **for** $(d_1, d_2) \in \mathcal{D}$ **do**
 - 2: Extract dimensions (d_1, d_2) of $\{\mathbf{x}_i\}_i \in \diamond$ to obtain $\{x_{i,d_1}, x_{i,d_2}\}_i$
 - 3: Calculate the convex hull on $\{x_{i,d_1}, x_{i,d_2}\}_i$, denoted by $\diamond_{(d_1, d_2)}$
 - 4: **end for**
 - 5: Sample cost $c \sim \text{Exp}(\sum_{(d_1, d_2) \in \mathcal{D}} L(\diamond_{(d_1, d_2)}))$
 - 6: **if** $c < \tau$ **then**
 - 7: Sample (d_1^*, d_2^*) from \mathcal{D} in proportion to $\{L(\diamond_{(1,2)}), \dots, L(\diamond_{(d-1,d)})\}$
 - 8: Sample θ, \mathbf{u} on the projection of the convex hull $\diamond_{(d_1^*, d_2^*)}$
 - 9: Use the new cutting hyperplane to generate two new convex hulls \diamond', \diamond''
 - 10: $\mathcal{V}' = \text{HullCut}(\diamond', \tau - c)$, $\mathcal{V}'' = \text{HullCut}(\diamond'', \tau - c)$
 - 11: Return $\{\diamond, C = \{c, (d_1^*, d_2^*), \theta, \mathbf{u}\}, \mathcal{V}', \mathcal{V}''\}$
 - 12: **else**
 - 13: Return $\{\diamond, \emptyset, \emptyset, \emptyset\}$
 - 14: **end if**
-

e. All previously existing level- l convex hulls in this branch are demoted to level- $(l+1)$ as a consequence of creating the new right level-1 convex hull.

- (iii) A new point f arrives outside the level-0 convex hull and the new generated cost value c' is larger than the current cost value c . The cut-line (red solid line) allocates the new point to the rightmost level-2 convex hull. Since this is a leaf node (no cut-lines inside), it forms a new level-2 convex hull including the new point (Lines 13 and 15, Algorithm 4).
- (iv) A new point g arrives inside the level-0 convex hull. Different levels of cutting lines are repeatedly compared to g until g is compared with a leaf node (Line 15, Algorithm 4). Since a larger budget τ_7 (i.e. the budget for 7 datapoints) is provided, new cuts may still be generated within the leaf node.

It is noted that Lines 2 ~ 3 in Algorithm 4 restrict a block

to be cut only if it contains more than 3 datapoints. If we have set an overly-large budget sequence, which prefers to generate small and trivial blocks, this restriction can help the algorithm avoid the overfitting issue.

Benefits of a convex hull representation: Cutting the full d -dimensional polyhedron generated from a series of cutting hyperplanes on the original domain is a challenging task. This is because completely indexing of this polyhedron requires extensive geometric manipulation, including calculating the intersection of multiple hyperplanes, determining if two hyperplanes intersect in the presence of other hyperplanes, and listing all vertices of the polyhedron.

Instead, implementing the hyperplane cut on the convex hull greatly simplifies these issues. The projection of the convex hull on any two dimensions can be simply obtained by extracting the elements of $\{\mathbf{x}_i\}_{i=1}^n$ in these dimensions, and then using a conventional convex hull detection algorithm (such as the Graham Scan algorithm [Graham, 1972] with a computational complexity of $\mathcal{O}(n \log n)$). Algorithm 6 describes the way of generating the hyperplane cut in a convex hull.

The self-consistency property (Theorem 1) of the BSP-Tree Process enables us conveniently and immediately have that:

Corollary 1. *The hyperplane restricted to the convex hull has the same distribution as if it was first generated on the “full” polyhedron, and then restricted to the convex hull.*

That is, the partitions of the BSP-Tree Process on the full space and on the data spanned convex hull will produce identical inferential outcomes.

Computational complexity: In the optimal case and assuming the BSP-Tree formed by the streaming data is a balanced tree (which keeps the height of trees in a complexity of $\log N$), the computational complex-

ity of a single BSP-Tree is $\mathcal{O}(N \log N \cdot d^2)$. When it is of the same magnitude as the $\mathcal{O}(N \log N \cdot d)$ of the Mondrian Forest [Lakshminarayanan et al., 2014, Lakshminarayanan et al., 2016] (also in the optimal case) in terms of N , the additional $\mathcal{O}(d)$ scaling factor is the price of more efficient cuts. In this perspective, this online BSP-Forest might be more suitable for low-dimensional regression/classification problems. In practice, we may alleviate this additional computational cost by using less hierarchical structure (through settings of smaller budget τ , see experiments in Section 5.3). The convex hull calculation is $\mathcal{O}(N \log N)$, which does not influence the general computational complexity.

In the worst case, when the height of the BSP-Tree equals to the number of datapoints (N) and each level has one split only, the computational complexity of the online BSP-Forest turns into $\mathcal{O}(N^2 d^2)$ (which is the same as the Mondrian Forest in terms of N). This complexity is still smaller than that of the batch version of a Random Forest ($\mathcal{O}(d \cdot N^2 \log N)$ [Lakshminarayanan et al., 2014, Lakshminarayanan et al., 2016]) in terms of N . It is also noted that the online BSP-Forest can be easily made to run in parallel as its component trees are updated in an independent manner.

When a new sample arrives, the computational complexity depends on the existing tree structure: if the BSP-tree is a balanced tree, the complexity is $\mathcal{O}(d^2 \log N)$; if the height of the BSP-tree equals to the number of existing samples (i.e., the worst case), the complexity is $\mathcal{O}(d^2 N)$.

In the memory usage part, the online BSP-Forest requires the same amount of $\mathcal{O}(Nd)$ as the Mondrian Forest. That is to say, each leaf node of the BSP-Tree would store all its belonging datapoints for future splitting.

Empirical label distribution: For the label distribution $p(y|\mathbf{x}, \mathcal{V}^{(0)})$, we use the empirical distribution of the labels from the training data to represent the label distribution on each of the leaf nodes. For classification tasks, we use a majority vote over the label predictions of each tree in the online BSP-Forest; for regression tasks, we use the mean value of the trees' label predictions at the given point. According to [Breiman, 2000, Biau et al., 2008, Mourta et al., 2017], this simple empirical approach usually performs competitively compared to constructing complex Bayesian models on the label distribution.

Universal consistency: As a larger value of the budget τ_n indicates a deeper tree structure and more complex partitions, the increasing budget sequence $\tau_{1:N}(\tau_{n+1} \geq \tau_n)$ indicates that the online BSP-Forest will produce more refined partitions with increasing amounts of data. This is consistent with the intuition behind, and a central tenet of, Bayesian nonparametrics. Similar observations (for Mondrian Forest only) has also been obtained in [Mourta et al., 2017]. Fur-

ther, it shows that such an increasing budget sequence is the key to guarantee the algorithm's performance converge to the optimal for all distributions over the labels and features.

More formally, let $\ell_n = P(g_n(\mathbf{x}) \neq y | \{(\mathbf{x}_i, y_i)\}_{i=1}^n)$ denote the error probability of these tree-structured online algorithm $g_n(\cdot)$. Using $\ell^* = \min_{g_n} \ell_n$ to denote the Bayesian error rate, which is generated by the optimal classifier. As the increasing budget with n results in finer partitions (i.e. more blocks and "smaller" block sizes), these online algorithms ensure there are a sufficiently large number of datapoints in each block, and its performance approaches the Bayesian error.

In order to discuss this "universal consistency" in the online BSP-Forest setting, we first investigate particular properties of an oblique line slice of the BSP-Tree Process.

Lemma 1. (Oblique line slice) *For any oblique line that crosses into the domain of a BSP-Tree Process with budget τ , its intersection points with the partition forms a homogeneous Poisson Process with intensity 2τ .*

Lemma 2 can enable us to describe basic characteristics (e.g. size, number) of the blocks of the BSP-Tree. Based on Lemma 2, the theoretical work of [Mourta et al., 2017] and Theorem 6.1 of [Devroye et al., 2013] and set restrictions on the budget sequence, we can obtain the resulting universal consistency for the online BSP-Forest as:

Theorem 2. *If $\lim_{n \rightarrow \infty} \tau_n \rightarrow \infty$ and $\lim_{n \rightarrow \infty} \frac{(\tau_n)^d}{n} \rightarrow 0$, then for classification tasks, we have $\lim_{n \rightarrow \infty} \mathbb{E}[\ell_n] \rightarrow \ell^*$.*

This universal consistency can be applied on any format of dataset as the result does not restrict the distribution of \mathbf{x} or the prediction function $g_n(\cdot)$.

Using the same proof techniques of [Mourta et al., 2017], we can obtain minimax convergence rate for the regression trees task as (the result for the classification trees can be obtained in a similar way):

Theorem 3. *Suppose that the label y is generated by a Lipschitz function $g(\cdot) : [0, 1]^d \rightarrow \mathbb{R}$ on the cubic space $[0, 1]^d$. Let $\hat{g}_n(\cdot)$ be an online BSP-Forest algorithm and that the budget sequence satisfies $\tau_n = \mathcal{O}(n^{1/(d+2)})$. Then, the following upper bound holds:*

$$\mathbb{E}_{\mathbf{x}} [(g(\mathbf{x}) - \hat{g}_n(\mathbf{x}))^2] = \mathcal{O}(n^{-2/(d+2)}) \quad (1)$$

for sufficiently large n , which corresponds to the minimax rate over the set of Lipschitz functions.

This result can be used for the guide of appropriately choosing the values on the budget sequence.

4 Related Work

Since its introduction in the early 2000s, the random forest [Breiman, 2001, Breiman, 2000] has become a state-of-the-art method for typical classification and regression tasks.

The literature is too vast to provide a comprehensive but compact survey, and so we focus on its online versions. For the frequentist-styled online random forest algorithms, they were developed by [Denil et al., 2013, Saffari et al., 2009, Domingos and Hulten, 2000]. The first two algorithms start from empty trees, and then grow the tree with more data based on evaluating a score function for each potential split position. As this score function relates to training performance, the node splitting procedure is label dependent. However, memory usage is inefficient in these two algorithms as the scores must be computed and stored for each potential split position. The third algorithm proposes to build online decision trees using constant memory and constant time per datapoint. These partitions are inefficient as only one feature is involved in the split procedure.

The Purely Random Forest (PRF) algorithm [Genuer, 2012, Arlot and Genuer, 2014] assumes tree generation is independent of data labels. When the split position is random, which is similar to the Mondrian Forest and the online BSP-Forest, the corresponding distribution on the resulting partition is not self-consistent. Further, its batch learning framework is not amenable to large-scale learning. [Genuer, 2012] proves that the PRF can achieve the minimax rate for estimating Lipschitz functions in the 1-dimensional case for single trees. [Arlot and Genuer, 2014] extends the analysis to forest settings and shows an improved convergence rate for smooth regression functions.

The Mondrian Forest [Lakshminarayanan et al., 2014, Lakshminarayanan et al., 2016] is the closest related method to the online BSP-Forest, as it uses the Mondrian process [Roy et al., 2007, Roy and Teh, 2009, Roy, 2011] to place a probability distribution over all the k -d-tree-based partitions of the domain. In regularising the Mondrian-Forest to be consistent, [Mourtada et al., 2017] sets the budget parameter to increase with the amount of data, and it then achieves the minimax rate in multi-dimensional space for single decision trees. [Mourtada et al., 2018] displays the advantage of Forest settings by showing improved convergence results.

In its favour, and in contrast to the above methods, the online BSP-Forest uses more than one dimension to implement node splits, and is accordingly more efficient. Further, the arrival of new data is dealt with by considering both the expansion of the feature space (i.e. the convex hull representation of tree nodes) and expansion of the budget line (i.e. an increasing budget sequence). This ensures the online BSP-Forest is represented efficiently and theoretically guaranteeing universal consistency.

5 Experiments

We examine the performance of the online BSP-Forest in regression and classification tasks. Unless specified, in each analysis, we re-scale the data features to the domain

$[0, 1]^d$ space, set the parameter of the Exponential distribution of cut cost to $L(\square)/2$ (half of the perimeter of the (2-dimensional) block \square), and specify the budget sequence as $\tau_n = n^{1/(d+2)} (\forall n \in \{1, \dots, N\})$. Through these experiments, we show that (1) the online-BSPF performs better than other online algorithms and at the same time, it keeps competitive to the batch trained algorithms in regression and classification tasks; (2) the online-BSPF produce more efficient partitions than the Mondrian Forest algorithm.

The online BSP-Forest is compared with several state-of-the-art methods: (1) a random forest (RF) [Breiman, 2001]; (2) Extremely Randomized Trees (ERT) [Geurts et al., 2006]; (3) a Mondrian Forest (MF) with fixed budget [Lakshminarayanan et al., 2014, Lakshminarayanan et al., 2016]; and (4) a Mondrian Forest with increasing budget [Mourtada et al., 2017]. The number of trees is fixed to $M = 100$ to avoid high computational costs. For the RF and ERT, we use the implementations in the `scikit-learn` toolbox [Pedregosa et al., 2011]. For the MF with infinite budget, we use the `scikit-garden` implementation. For the parameter tuning in the RF and ERT, we use the `GridSearchCV` package in the `scikit-learn` toolbox and focus on tuning the features of “`max_features`”, which concerns the number of features considered when selecting the best split. Each test case was replicated 16 times, and we report summary means and $1.96 \times$ standard errors for each measure.

5.1 Classification

We examine the classification accuracy of the online BSP-Forest through four real datasets [Chang and Lin, 2011] used in [Lakshminarayanan et al., 2016, Denil et al., 2013]: `satimages` ($N = 4,435$), `letter` ($N = 15,000$), `dna` ($N = 2,000$) and `usps` ($N = 7,291$). For all these 4 datasets, we use Principle Component Analysis (PCA) to extract 4 principle components before deploying the models. As we have mentioned that the online BSP-Forest is suitable for low dimensional case, this dimensional reduction technique helps us to largely reduce the computational cost (e.g. DNA dataset with 256 features). For each dataset, we use different ratios of the whole data as the training data and use the rest as the testing data. For the label prediction, we would first use the majority vote to determine the class label of the nodes in each tree and then again use the majority vote over the datapoints’ covered nodes to predict the label for the data point.

The detail classification performance (under different ratios of training data) for each dataset is displayed in Figure 3. Except for the `dna` dataset, the performance of the online-BSPF is quite competitive to RF and ERT and much better than the Mondrian Forest algorithm in other three datasets. As RF, ERT and MF proceed each cut using one feature only, the effectiveness of oblique cuts can be verified even

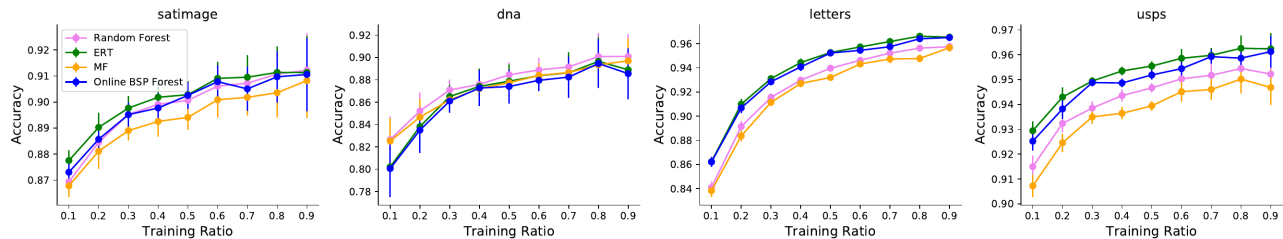


Figure 3: Classification accuracy (± 1.96 standard error) for the satimage, dna, letters and usps datasets. The x -axis indicates to the ratio of training:testing data.

Table 1: Performance comparison on Apartment data and Airline data (RMSE ± 1.96 standard error)

Dataset	RF	ERT	MF (fixed τ)	MF (increasing τ_n)	online BSP-Forest
Apartment	0.526 \pm 0.02	0.531 \pm 0.02	0.545 \pm 0.04	0.541 \pm 0.03	0.536 \pm 0.03
Airline (100K)	32.2 \pm 0.7	34.1 \pm 1.0	36.5 \pm 0.5	35.1 \pm 1.2	35.9 \pm 0.8
Airline (400K)	33.7 \pm 0.4	33.5 \pm 0.9	35.8 \pm 1.2	36.2 \pm 0.9	35.2 \pm 1.3
Airline (1M)	34.1 \pm 0.9	33.5 \pm 0.6	37.3 \pm 1.1	36.5 \pm 0.6	35.9 \pm 1.1

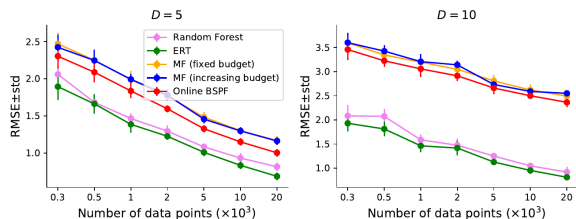


Figure 4: RMSE (± 1.96 standard error) on Friedman’s test function, as a function of the number of training data (x -axes) and dimension of the features \mathbf{x} .

for the online setting.

5.2 Regression

Friedman’s Function (simulated data): The performance of the online BSP-Forest is first evaluated on the Friedman’s function [Friedman, 1991, Chipman et al., 2010, Linero and Yang, 2017]. In this setting, each datapoint $\mathbf{x}' = (x_1, \dots, x_d)$ is generated from a d -dimensional uniform distribution, and its label y takes the form:

$$y = 10 \sin(\pi x_1 x_2) + 20 \left(x_3 - \frac{1}{2} \right)^2 + 10x_4 + 5x_5 + \epsilon \quad (2)$$

, where $\epsilon \sim \mathcal{N}(0, \sigma^2)$, $\sigma^2 = 1$. Friedman’s function consists of two nonlinear terms, two linear terms and an interaction term.

We compute the RMSE (root mean squared error) under each method as the true function is known, for different numbers of datapoints N , and for two different dimensional setups: $d = 5$ where all dimensions are informative, and $d = 10$ where only the first 5 dimensions are informative. The results are shown in Figure 8. The online BSP-Forest

performs better (in RMSE) than the two (online) Mondrian-Forests, with ~ 0.1 improvement in RMSE.

Since the three online algorithms are implemented independently of the data labels, it is not surprising that they perform worse than the batch trained RF and ERT. The performance differential is greater when 5 noisy dimensions ($d = 10$) are added. Because the online-BSPF purely uses the generative process to generate the tree structure, it distinguishes between meaningful and noisy dimensions less well. Similar observations have been reported in [Lakshminarayanan et al., 2016]. We may overcome such a performance deficit by increasing the budget, which will permit additional cuts in meaningful dimensions in spite of some less useful cuts in noisy dimensions.

UK Apartment Price data: The performance of the online BSP-Forest is examined on the UK Apartment Price Data [Hensman et al., 2013], which records the selling price of 122,341 apartments in the UK from February to October 2012. We take the apartment price as the target label data, and use GPS coordinates (coarsely estimated based on the apartment’s postcode and GPS database) as the feature data (\mathbf{x}).

To evaluate the performance of the online BSP-Forest, we randomly sample 20% of the data as the training data and predict the price values on the remaining data. Row 1 in Table 1 displays the RMSE values of each method. While, as before, the RF and ERT methods perform better than the three online learning algorithms, their RMSE values are similar. Also, the online BSP-Forest outperforms the more directly comparable Mondrian Forest variants.

Airline Delay data: We finally analyse the regression performance of the online BSP-Forest on

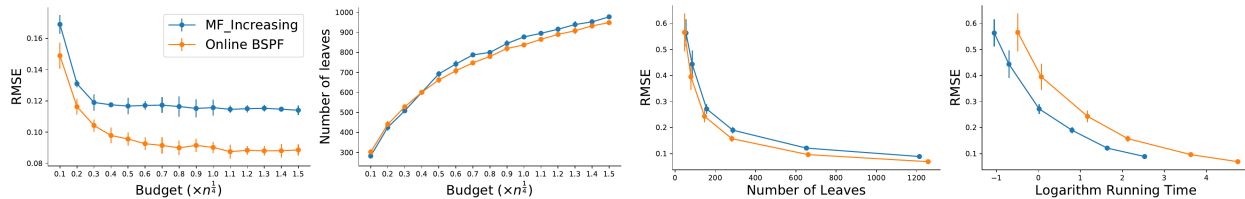


Figure 5: Left two sub-figures: RMSE and number of leaf nodes comparisons for the Mondrian Forest and the online BSP-Forests under different settings of the budget sequences. Right two sub-figures: RMSE comparison under different number of datapoints. Points in each curve refers to the case of $N = 300, 500, 1,000, 2,000, 5,000, 10,000$ datapoints.

the airline delay data [Hensman et al., 2013]. We wish to predict flight delay time (y) based on 8 factors (\mathbf{x}). Following [Deisenroth and Ng, 2015, Lakshminarayanan et al., 2016], these factors are set to include the age of the plane, prospective flight distance, prospective flight airtime, departure time, arrival time, day of the week, day of the month and month of the year.

Following the settings of [Deisenroth and Ng, 2015, Lakshminarayanan et al., 2016], we set the number of training datapoints as $N = 100K, 400K$ and 1 million, and specify the test data as the $100K$ observations immediately following the training data. Rows 2–4 in Table 1 display each methods’ RMSE values. Similar conclusions can be drawn as for the previous analyses: while the RF and ERT perform better than any the online algorithm, the online BSP-Forest is the best performing online algorithm. In the exceptional case of $N = 100K$, where the MF with increasing budget performs better than the online BSP-Forest, the former variance (1.2) is larger than the later (0.8).

5.3 Efficiency of the cutting strategy

Cutting efficiency is a primary advantage of the online BSP-Forest. We quantitatively explore this efficiency issue through the simple function: $y = 10 \sin(\pi x_1 x_2) + 0.2\epsilon$, $\epsilon \sim \mathcal{N}(0, 1)$. Two different cases are investigated: (1) different budget sequences. We set $N = 5,000$ and the budget sequence as $\tau_n = 0.1n^{1/4}, 0.2n^{1/4}, \dots, 1.5n^{1/4}$; (2) different number of datapoints. Based on the results of case (1), we set $\tau_n = n^{1/4}$ and let the number of datapoints as $N = 300, 500, 1,000, 2,000, 5,000, 10,000$ for case (2). Performance results are shown in Figure 5.

For case (1), the left two sub-figures confirm that, for different budget sequences, the online BSP-Forest can always obtain better RMSE performance than the Mondrian Forest. The numbers of leaves are also similar between these two algorithms. It is noted that, as each node is restricted to be cut only if it contains more than 3 datapoints, these algorithms’ performance becomes stable even for large value settings of budget sequences. For case (2), the right two sub-figures indicate the consistent better performance of the online-BSPF for different number of datapoints, with

the price of requiring a bit longer running time (due to the computational cost of $\mathcal{O}(d^2)$).

6 Conclusion & Future work

In this paper we have developed an online BSP-Forest framework that addresses the scalability and theoretical challenges of the online BSP-Forest algorithm. Through a non-trivial scheme for efficiently incorporating sequential datapoints, the model construction for the online BSP-Forest follows the same distribution as that for the batch setting. By using more than one dimension to cut the underlying space, the online BSP-Forest is a demonstrably efficient model for classification and regression tasks. Our experimental results (Section 5) verify that the online BSP-Forest consistently outperforms the Mondrian-Forest, and is competitive with other batch random forest models.

For the future work, the Random Tessellation Forest [Ge et al., 2019] has extended the BSP-Tree Process by generating arbitrary sloped cutting hyperplanes in d -dimensional spaces. Extending the Random Tessellation Forest to the online learning setting and comparing with the online BSP-Forest would be interesting work. Recently, [O’Reilly and Tran, 2020] uses the technique of iteration stable (STIT) tessellations to efficiently generate arbitrary sloped cuts. It might be possible to use their method to further reduce the $\mathcal{O}(d^2)$ factor to the computational cost of the online BSP-Forest and make the online BSP-Forest suitable for high-dimensional data as well.

Acknowledgements

Xuhui Fan and Scott A. Sisson are supported by the Australian Research Council through the Australian Centre of Excellence in Mathematical and Statistical Frontiers (ACEMS, CE140100049), and Scott A. Sisson through the Discovery Project Scheme (DP160102544). Bin Li is supported by Shanghai Municipal Science & Technology Commission (16JC1420401) and the Program for Professor of Special Appointment (Eastern Scholar) at Shanghai Institutions of Higher Learning.

References

- [Airoldi et al., 2009] Airoldi, E., Blei, D., Fienberg, S., and Xing, E. (2009). Mixed membership stochastic block-models. In *NIPS*, pages 33–40.
- [Arlot and Genuer, 2014] Arlot, S. and Genuer, R. (2014). Analysis of purely random forests bias. *arXiv preprint arXiv:1407.3939*.
- [Balog and Teh, 2015] Balog, M. and Teh, Y. W. (2015). The mondrian process for machine learning. *arXiv preprint arXiv:1507.05181*.
- [Biau et al., 2008] Biau, G., Devroye, L., and Lugosi, G. (2008). Consistency of random forests and other averaging classifiers. *Journal of Machine Learning Research*, 9(Sep):2015–2033.
- [Breiman, 2000] Breiman, L. (2000). Some infinity theory for predictor ensembles. Technical report, Technical Report 579, Statistics Dept. UCB.
- [Breiman, 2001] Breiman, L. (2001). Random forests. *Machine Learning*, 45(1):5–32.
- [Chang and Lin, 2011] Chang, C.-C. and Lin, C.-J. (2011). Libsvm: A library for support vector machines. *ACM Trans. Intell. Syst. Technol.*, 2(3):27:1–27:27.
- [Chipman et al., 2010] Chipman, H. A., George, E. I., and McCulloch, R. E. (2010). Bart: Bayesian additive regression trees. *The Annals of Applied Statistics*, 4(1):266–298.
- [Crane, 2012] Crane, H. (2012). *Infinitely Exchangeable Partition, Tree and Graph-valued Stochastic Processes*. PhD thesis.
- [Deisenroth and Ng, 2015] Deisenroth, M. P. and Ng, J. W. (2015). Distributed Gaussian processes. In *ICML*, pages 1481–1490.
- [Denil et al., 2013] Denil, M., Matheson, D., and Freitas, N. (2013). Consistency of online random forests. In *ICML*, volume 28, pages 1256–1264.
- [Devroye et al., 2013] Devroye, L., Györfi, L., and Lugosi, G. (2013). *A probabilistic theory of pattern recognition*, volume 31. Springer Science & Business Media.
- [Domingos and Hulten, 2000] Domingos, P. and Hulten, G. (2000). Mining high-speed data streams. In *Kdd*, volume 2, page 4.
- [Fan et al., 2019a] Fan, X., Li, B., Sisson, S., Li, C., and Chen, L. (2019a). Scalable deep generative relational model with high-order node dependence. In *NeurIPS*, pages 12637–12647.
- [Fan et al., 2018a] Fan, X., Li, B., and Sisson, S. A. (2018a). The binary space partitioning-tree process. In *AISTATS*, volume 84 of *Proceedings of Machine Learning Research*, pages 1859–1867.
- [Fan et al., 2018b] Fan, X., Li, B., and Sisson, S. A. (2018b). Rectangular bounding process. In *NeurIPS*, pages 7631–7641.
- [Fan et al., 2019b] Fan, X., Li, B., and Sisson, S. A. (2019b). Binary space partitioning forests. In *AISTATS*, volume 89, pages 3022–3031.
- [Fan et al., 2016a] Fan, X., Li, B., Wang, Y., Wang, Y., and Chen, F. (2016a). The Ostomachion Process. In *AAAI Conference on Artificial Intelligence*, pages 1547–1553.
- [Fan et al., 2016b] Fan, X., Xu, R. Y. D., and Cao, L. (2016b). Copula mixed-membership stochastic block model. In *IJCAI*.
- [Friedman, 1991] Friedman, J. H. (1991). Multivariate adaptive regression splines. *The Annals of Statistics*, 19:1–67.
- [Ge et al., 2019] Ge, S., Wang, S., Teh, Y. W., Wang, L., and Elliott, L. (2019). Random tessellation forests. In *NeurIPS*, pages 9571–9581.
- [Genuer, 2012] Genuer, R. (2012). Variance reduction in purely random forests. *Journal of Nonparametric Statistics*, 24(3):543–562.
- [Geurts et al., 2006] Geurts, P., Ernst, D., and Wehenkel, L. (2006). Extremely randomized trees. *Machine learning*, 63(1):3–42.
- [Graham, 1972] Graham, R. L. (1972). An efficient algorithm for determining the convex hull of a finite planar set. *Information Processing Letters*, 1(4):132–133.
- [Hensman et al., 2013] Hensman, J., Fusi, N., and Lawrence, N. D. (2013). Gaussian processes for big data. In *UAI*, pages 282–290.
- [Karrer and Newman, 2011] Karrer, B. and Newman, M. E. (2011). Stochastic blockmodels and community structure in networks. *Physical Review E*, 83(1):016107.
- [Kemp et al., 2006] Kemp, C., Tenenbaum, J. B., Griffiths, T. L., Yamada, T., and Ueda, N. (2006). Learning systems of concepts with an infinite relational model. In *AAAI*, volume 3, pages 381–388.
- [Lakshminarayanan et al., 2014] Lakshminarayanan, B., Roy, D. M., and Teh, Y. W. (2014). Mondrian forests: Efficient online random forests. In *NIPS*, pages 3140–3148.

- [Lakshminarayanan et al., 2016] Lakshminarayanan, B., Roy, D. M., and Teh, Y. W. (2016). Mondrian forests for large-scale regression when uncertainty matters. In *AISTATS*, pages 1478–1487.
- [Li et al., 2009] Li, B., Yang, Q., and Xue, X. (2009). Transfer learning for collaborative filtering via a rating-matrix generative model. In *ICML*, pages 617–624.
- [Linero and Yang, 2017] Linero, A. R. and Yang, Y. (2017). Bayesian regression tree ensembles that adapt to smoothness and sparsity. *arXiv preprint arXiv:1707.09461*.
- [Mourtada et al., 2017] Mourtada, J., Gaïffas, S., and Scornet, E. (2017). Universal consistency and minimax rates for online mondrian forests. In *NIPS*, pages 3758–3767.
- [Mourtada et al., 2018] Mourtada, J., Gaïffas, S., and Scornet, E. (2018). Minimax optimal rates for mondrian trees and forests. *arXiv preprint arXiv:1803.05784*.
- [Nakano et al., 2014] Nakano, M., Ishiguro, K., Kimura, A., Yamada, T., and Ueda, N. (2014). Rectangular tiling process. In *ICML*, pages 361–369.
- [Nowicki and Snijders, 2001] Nowicki, K. and Snijders, T. A. (2001). Estimation and prediction for stochastic block structures. *Journal of the American Statistical Association*, 96(455):1077–1087.
- [O’Reilly and Tran, 2020] O’Reilly, E. and Tran, N. (2020). Stochastic geometry to generalize the mondrian process. *arXiv preprint arXiv:2002.00797*.
- [Pedregosa et al., 2011] Pedregosa, F., Varoquaux, G., Gramfort, A., Michel, V., Thirion, B., Grisel, O., Blondel, M., Prettenhofer, P., Weiss, R., Dubourg, V., et al. (2011). Scikit-learn: Machine learning in Python. *Journal of Machine Learning Research*, 12(Oct):2825–2830.
- [Porteous et al., 2008] Porteous, I., Bart, E., and Welling, M. (2008). Multi-HDP: A non parametric Bayesian model for tensor factorization. In *AAAI*, pages 1487–1490.
- [Roy, 2011] Roy, D. M. (2011). *Computability, Inference and Modeling in Probabilistic Programming*. PhD thesis, MIT.
- [Roy et al., 2007] Roy, D. M., Kemp, C., Mansinghka, V., and Tenenbaum, J. B. (2007). Learning annotated hierarchies from relational data. In *NIPS*, pages 1185–1192.
- [Roy and Teh, 2009] Roy, D. M. and Teh, Y. W. (2009). The Mondrian process. In *NIPS*, pages 1377–1384.
- [Saffari et al., 2009] Saffari, A., Leistner, C., Santner, J., Godec, M., and Bischof, H. (2009). On-line random forests. In *ICCV Workshops*, pages 1393–1400.

[Yule, 1925] Yule, G. U. (1925). A mathematical theory of evolution based on the conclusions of Dr. Jc Willis, FRS. *Philosophical Transactions of the Royal Society B*.

A Algorithm of Generating A Cut in \diamond' and Not Crossing into \diamond

Algorithm 6 GenCutNorCross(\diamond', \diamond)

- 1: $(d_1^*, d_2^*) \sim \text{Cat}(\tilde{L}_{(1,2)}(\diamond') - \tilde{L}_{(1,2)}(\diamond), \dots, \tilde{L}_{(d-1,d)}(\diamond') - \tilde{L}_{(d-1,d)}(\diamond))$
 - 2: $\theta \sim p(\theta) \propto |\mathbf{l}_{\Pi_{(d_1^*, d_2^*)}(\diamond')}(\theta)| - |\mathbf{l}_{\Pi_{(d_1^*, d_2^*)}(\diamond)}(\theta)|, \theta \in (0, \pi]$
 - 3: Sample \mathbf{u} uniformly on $|\mathbf{l}_{\Pi_{(d_1^*, d_2^*)}(\diamond')}(\theta)| - |\mathbf{l}_{\Pi_{(d_1^*, d_2^*)}(\diamond)}(\theta)|$
 - 4: Form cutting hyperplane based on $(d_1^*, d_2^*), \theta, \mathbf{u}$
-

B Some visualisations

Left panel of Figure 6 visualizes the difference between the convex hull representation of tree node in the BSP-Tree partition and Mondrian tree partition. Convex hulls are formed recursively, and larger hulls contain smaller ones. The BSP-Tree generates smaller convex hulls than the Mondrian-Tree, which means the BSP-Tree is a “tight” representation of the space. Right panel of Figure 6 visualizes oblique line slice of the BSP-Tree Process.

C Proof of Lemma 1

Lemma 2. (*Oblique line slice*) For any oblique line that crosses into the domain of a BSP-Tree process with budget τ , its intersection points with the partition forms a homogeneous Poisson process with intensity 2τ .

Proof. The self-consistent property of the BSP-Tree process guarantees that this 1-dimensional slice follows the same way of directly generating a BSP-Tree partition on the line.

To define the BSP-Tree partition on the line segment, we first consider the BSP-Tree partition in an obtuse triangle. Two vertices of the triangle form a line segment with the length L . Another vertex lies between these two vertices and has an ϵ distance to the line segment. Based on the generative process of the BSP-Tree process, the cost of cut in this triangle follows an Exponential distribution with rate parameter being the perimeter of the triangle, which is $PE = (L_1 + L_2) + \sqrt{L_1^2 + \epsilon^2} + \sqrt{L_2^2 + \epsilon^2}$. As $PE \rightarrow 2(L_1 + L_2)$ when $\epsilon \rightarrow 0$, the cost has an exponential distribution with rate parameter $2L$ accordingly. As a result, the number of cuts follows a Poisson distribution with parameter $\tau \cdot 2L$. The cut position is Uniformly distributed in the line segment. (For each projection in the direction

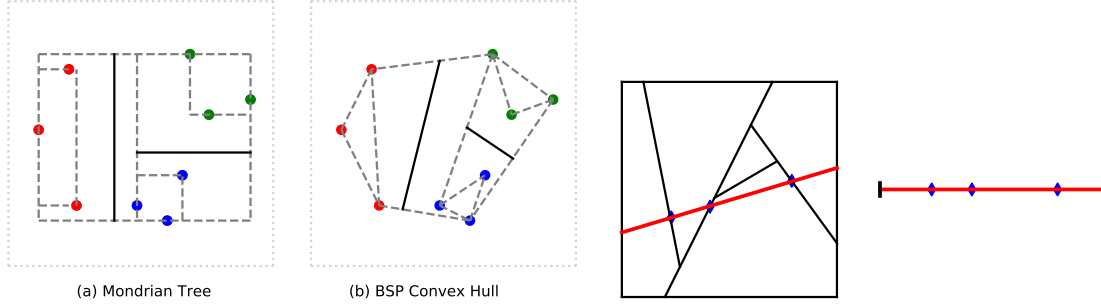


Figure 6: Left: example visualization comparing the Mondrian-Tree and BSP-Tree convex hulls. Point colors identify different data labels, and the dotted, dashed and solid lines denote the whole space, the convex hulls and the cuts, respectively. Right: $2d$ visualization of oblique line slice of the BSP-Tree Process partition. Red solid line denotes the oblique line and blue dots represents the intersection points.

of θ , the crossing point between the cuts and line segment is Uniformly distributed.) This can verify the independent increments of the partition points in the line.

As the two condition of Poisson process is satisfied, according to Theorem 1.10 in [Balog and Teh, 2015], we can get the conclusion. \square

D Proof of Theorem 2

It is noted the main idea of the following proof largely follows the work of [Mourtada et al., 2017]. We make modifications to make the proof suitable to online BSP-Forest case.

Lemma 3. (Block diameter) Let $\mathbf{x} \in [0, 1]^d$, and let $D(\mathbf{x})$ be the L^2 -diameter of the block containing \mathbf{x} in the BSP-Tree partition with budget $\tau/2$. If $\tau \rightarrow \infty$, then $D_\tau(\mathbf{x}) \rightarrow 0$ in probability. More precisely, for every $\delta, \tau > 0$, we have

$$\mathbb{P}(D_\tau(\mathbf{x}) \geq \delta) \leq d(1 + \frac{\tau\delta}{\sqrt{d}}) \exp(-\frac{\tau\delta}{\sqrt{d}}), \quad \mathbb{E}[D_\tau(\mathbf{x})^2] \leq \frac{4d}{\tau^2}.$$

Proof. Let $\square_\tau(\mathbf{x})$ denotes the block of a Binary Space Partitioning-Tree partition containing $\mathbf{x} \in [0, 1]^d$. In the space of $[0, 1]^d$, we can build up d orthogonal bases to describe the block $\square_\tau(\mathbf{x})$, with one basis is in the direction of largest diameter in $\square_\tau(\mathbf{x})$. While it is obvious that rotations of the block will not affect the diameter, w.l.o.g., we rotate the block and treat the direction with largest diameter as dimension 1. By definition, the L^∞ -norm diameter $D_\tau(\mathbf{x})$ of $\square_\tau(\mathbf{x})$ is $\max\{\square_\tau^{(d')}(\mathbf{x})\}_{d'}$. While recording these smallest and largest interceptions in these rotated dimensions as $\{L_\tau^{(d')}, R_\tau^{(d')}\}_{d'}$, all of the random variables $R_\tau(\mathbf{x}) - L_\tau(\mathbf{x})$ have the same distribution, it suffices to consider $D_\tau^{(1)}(\mathbf{x}) = R_\tau^{(1)}(\mathbf{x}) - L_\tau^{(1)}(\mathbf{x})$.

In this rotated block, consider the segment $I^{(1)}(\mathbf{x}) = [0, \sqrt{d}] \times \mathbf{x}^{-i}$ containing \mathbf{x} , and denote $\phi_\tau^1(\mathbf{x}) \subset [0, \sqrt{d}]$

the restriction of the partition to $I^{(1)}(\mathbf{x})$. Note that $R_\tau^{(1)}(\mathbf{x})$ ($L_\tau^{(1)}(\mathbf{x})$) is the lowest (highest) element of $\phi_\tau^1(\mathbf{x})$ that is larger (smaller) than x_1 , and is equal to \sqrt{d} (0) if $\phi_\tau^1(\mathbf{x}) \cap [x_1, \sqrt{d}]$ ($\phi_\tau^1(\mathbf{x}) \cap [0, x_1]$) is empty. By Theorem 1 and Lemma 1, $\phi_\tau(\mathbf{x})$ is a Poisson process with intensity τ .

This implies the distribution of $(L_\tau^{(1)}(\mathbf{x}), R_\tau^{(1)}(\mathbf{x}))$ is the same as that of $(\tilde{L}_\tau^{(1)}(\mathbf{x}) \vee 0, \tilde{R}_\tau^{(1)}(\mathbf{x}) \wedge \sqrt{d})$, where $\tilde{\phi}_\tau^1(\mathbf{x})$ is a Poisson process on \mathbb{R} with intensity τ , and $\tilde{L}_\tau^{(1)}(\mathbf{x}) = \sup(\tilde{\phi}_\tau^1(x_1) \cup (-\infty, x_1))$, $\tilde{R}_\tau^{(1)}(\mathbf{x}) = \inf(\tilde{\phi}_\tau^1(x_1) \cap (x_1, \infty))$. By the property of the Poisson point process, this implies that $x_1 - L_\tau^{(1)}(\mathbf{x}), R_\tau^{(1)}(\mathbf{x}) - x_1 \stackrel{d}{=} (E_1, E_2)$, where E_1, E_2 are independent exponential random variables with parameter τ . $D_\tau^{(1)}(\mathbf{x}) = R_\tau^{(1)}(\mathbf{x}) - x_1 + x_1 - L_\tau^{(1)}(\mathbf{x})$ is upper bounded by $E_1 + E_2 \sim \text{Gamma}(2, \tau)$. Thus, we have $\forall \delta > 0, \mathbb{P}(D_\tau^{(1)}(\mathbf{x}) \geq \delta) \leq (1 + \tau\delta)e^{-\tau\delta}$ and $\mathbb{E}[D_\tau^{(1)}(\mathbf{x})^2] \leq \mathbb{E}(E_1^2) + \mathbb{E}(E_2^2) = \frac{4}{\tau^2}$. The bound of $D_\tau(\mathbf{x})$ can be obtained by $D_\tau(\mathbf{x}) = \sqrt{\sum_{d'} D_\tau^{(d')}(\mathbf{x})}$. \square

Lemma 4. If K_τ denotes the number of cuts in the BSP-Tree process, we have $\mathbb{E}[K_\tau] \leq (1 + \tau)^d e^{d(d-1)}$.

Proof. Let $\square \subset [0, 1]^d$ be an arbitrary block, and let K_τ^\square denotes the number of splits performed in the BSP-Tree process with budget value $\tau/2$. As shown in [Fan et al., 2018a][Fan et al., 2019b], the waiting time of a cut occurs in a leaf node ϕ of the BSP-Tree process follows an exponential distribution of rate $L(\square_\phi) \leq L(\square)$, where $L(\square)$ denotes the perimeter of the block \square . The number of leaves $K_t + 1 \geq K_t$ at time t is dominated by the number of individuals in a Yule process with rate $L(\square)$ [Yule, 1925]. Thus, we have: $\mathbb{E}(K_\tau^\square) \leq e^{\tau L(\square)}$.

Considering the covering \mathcal{C} of \square by a regular grid of $\lceil \tau \rceil^d$ boxes obtained by equally dividing each coordinate of \square in $\lceil \tau \rceil$ parts. Each cut in \square will induce a split in at least one box C in \mathcal{C} and B_τ^C is also a BSP-Tree process in box C (due to the self-consistency of the BSP-Tree process),



Figure 7: Visualization for the 1-dimensional space case.

we have: $\mathbb{E}(K_\tau^\square) \leq \sum_{C \in \mathcal{C}} \mathbb{E}(K_\tau^C) \leq \lceil \tau \rceil^d e^{\tau \frac{L(\square)}{\tau}} \leq (\tau + 1)^d e^{L(\square)}$. \square

Lemma 5. *Assume that the total number of splits K_τ performed by the BSP-Tree partition satisfies $\lim_{n \rightarrow \infty} \mathbb{E}(K_{\tau_n})/n \rightarrow 0$. For $N_n(\mathbf{x})$ being the number of datapoints in $\mathbf{x}_{1:N}$ fall in $A_{\tau_n}(\mathbf{x})$, we have $N_n(\mathbf{x}) \rightarrow \infty$ in probability.*

Proof. We fix $n \geq 1$, and conditionally on the BSP-Tree partition at the budget of τ_n , B_{τ_n} is independent of \mathbf{x} by construction. Note that the number of leaves is $|\mathcal{L}(B_{\tau_n})| = K_{\tau_n} + 1$, and $(\square_\phi)_{\phi \in \mathcal{L}(B_{\tau_n})}$ is the corresponding blocks, where ϕ refers to the leaf node. For ϕ , we define N_ϕ to be the number of points among $\mathbf{x}_1, \dots, \mathbf{x}_n$ that fall in the cell \square_ϕ . Since $\mathbf{x}_1, \dots, \mathbf{x}_n$ are i.i.d., so that the joint distribution of $\mathbf{x}_1, \dots, \mathbf{x}_n$ is invariance under the permutation of the $n + 1$ datapoints, conditionally on the set $S = \mathbf{x}_1, \dots, \mathbf{x}_n$ the probability that \mathbf{x} falls in the block \square_ϕ . Therefore, for each $t > 0$, we have:

$$\begin{aligned} \mathbb{P}(N_n(\mathbf{x}) \leq t) &= \mathbb{E}\{\mathbb{P}(N_n(\mathbf{x}) \leq t | S, B_{\tau_n})\} \\ &= \mathbb{E}\left\{ \sum_{\phi \in \mathcal{L}(B_{\tau_n}): N_\phi \leq t} \frac{N_\phi}{n+1} \right\} \quad (3) \\ &\leq \mathbb{E}\left\{ \frac{t |\mathcal{L}(B_{\tau_n})|}{n+1} \right\} = \frac{t(\mathbb{E}(K_{\tau_n}) + 1)}{n+1} \end{aligned}$$

which tends to 0 as $n \rightarrow \infty$. \square

Before proving Theorem 2, we first invoke a consistency theorem (Theorem 6.1 in [Devroye et al., 2013] and we use \square to denote the block for notation consistency)

Theorem 4. *Consider a sequence of randomised tree classifiers $(\hat{g}_n(\cdot, Z))$, grown independently of the labels Y_1, \dots, Y_n . For $\mathbf{x} \in [0, 1]^d$, denote $\square_n(\mathbf{x}) = \square_n(\mathbf{x}, Z)$ the block containing \mathbf{x} , $D_n(\mathbf{x})$ its diameter and $N_n(\mathbf{x}) = N_n(\mathbf{x}, Z)$ the number of input vectors among $\mathbf{x}_1, \dots, \mathbf{x}_n$ that fall in $\square_n(\mathbf{x})$. Assume that, if \mathbf{x} is drawn from the distribution with the following conditions:*

1. $\lim_{n \rightarrow \infty} D_n(\mathbf{x}) \rightarrow 0$ in probability;
2. $\lim_{n \rightarrow \infty} N_n(\mathbf{x}) \rightarrow \infty$ in probability.

Then the tree classifier \tilde{g}_n is consistent.

The proof of Theorem 2 is:

Proof. We can show the two conditions in Theorem 4 are satisfied. First, Lemma 1 ensures that, if $\tau_n \rightarrow \infty$, $D_{\tau_n}(\mathbf{x}) \rightarrow 0$ in probability for every $\mathbf{x} \in [0, 1]^d$. In particular, for every $\delta > 0$, we have $\mathbb{P}(\square_{\tau_n}(\mathbf{x}) \geq \delta) = \int_{[0, 1]^d} \mathbb{P}(D_{\tau_n}(\mathbf{x}) > \delta) \mu(d\mathbf{x}) \rightarrow 0$ as $n \rightarrow \infty$ by the dominated convergence theorem.

Since Lemma 5 provides the proof for the second condition, the proof of Theorem 2 is concluded. \square

E Proof of Theorem 3

It is noted the main idea of the following proof largely follows the work of [Mourtada et al., 2017]. We make modifications to make the proof suitable to online BSP-Forest case.

Proof. By the convexity of the quadratic loss function and the fact that all the BSP-Tree has the same distribution, we have that $\mathbb{E}[(g(\mathbf{x}) - \hat{g}_n(\mathbf{x}))^2] \leq \frac{1}{m} \sum_{k=1}^m \mathbb{E}[(g(\mathbf{x}) - \hat{g}_{n,k}(\mathbf{x}))^2] = \mathbb{E}[(g(\mathbf{x}) - \hat{g}_{n,1}(\mathbf{x}))^2]$. Thus, we can prove the result for a single tree algorithm to get the conclusion. \square

We first write use the bias-variance decomposition of the quadratic loss by:

$$R(\hat{f}_n) = \mathbb{E}[(f(\mathbf{x}) - \bar{f}_n(\mathbf{x}))^2] + \mathbb{E}[(\hat{f}_n(\mathbf{x}) - \bar{f}_n(\mathbf{x}))^2] \quad (4)$$

where $\bar{f}_n(\mathbf{x}) := \mathbb{E}[f(\mathbf{x}) | \mathbf{x} \in A_n(\mathbf{x})]$ denotes the groundtruth label value for the block containing \mathbf{x} . The first term is bias and it measures the closeness of $f(\mathbf{x})$ to the best approximator $\bar{f}_n(\mathbf{x})$ (of which the label value is constant on the block containing \mathbf{x}). The second term is variance and it measures the closeness of the best approximator $\bar{f}_n(\mathbf{x})$ to the empirical approximator $\hat{f}_n(\mathbf{x})$.

For the bias term, we have:

$$\begin{aligned} |f(\mathbf{x}) - \bar{f}_n(\mathbf{x})| &\leq \left| \frac{1}{\mu(A_n(\mathbf{x}))} \int_{A_n(\mathbf{x})} (f(\mathbf{x}) - \bar{f}_n(\mathbf{z})) \mu(d\mathbf{z}) \right| \\ &\leq \sup_{\mathbf{z} \in A_n(\mathbf{x})} |f(\mathbf{x}) - f(\mathbf{z})| \\ &\leq L \sup_{\mathbf{z} \in A_n(\mathbf{x})} \|\mathbf{x} - \mathbf{z}\|_2 = L \cdot D_n(\mathbf{x}) \quad (5) \end{aligned}$$

where $D_n(\mathbf{x})$ is the l^2 -diameter of $A_n(\mathbf{x})$. According to the result of Lemma 1, we get:

$$\mathbb{E}[(f(\mathbf{x}) - \bar{f}_n(\mathbf{x}))^2] \leq L^2 \mathbb{E}[D_n(\mathbf{x})^2] \leq \frac{4dL^2}{\tau_n^2} \quad (6)$$

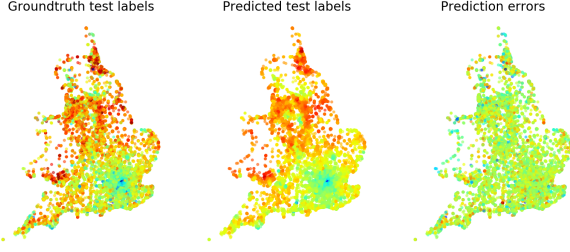


Figure 8: Visualisation of the online BSP-Forest’s spatial predictions on the UK Apartment Price data. Plots show [L-R] actual test data, predictions, and prediction errors. Red–blue colour denotes low–high prices.

For the variance term, based on the Proposition 2 of [Arlot and Genuer, 2014]: if U is a random tree partition of the unit space with $k + 1$ blocks, we have:

$$\mathbb{E} \left[(\bar{f}_U(\mathbf{x}) - \hat{f}_U(\mathbf{x}))^2 \right] \leq \frac{k+1}{n} (2\sigma^2 + 9\|f\|_\infty) \quad (7)$$

. Thus, we can have:

$$\begin{aligned} \mathbb{E} \left[(\bar{f}_n(\mathbf{x}) - \hat{f}_n(\mathbf{x}))^2 \right] &= \sum_{k=0}^{\infty} \mathbb{P}(k) \mathbb{E} \left[(\bar{f}_U(\mathbf{x}) - \hat{f}_U(\mathbf{x}))^2 | k \right] \\ &\leq \sum_{k=0}^{\infty} \mathbb{P}(k) \frac{k+1}{n} (2\sigma^2 + 9\|f\|_\infty) \\ &= \frac{\mathbb{E}(K_n) + 1}{n} (2\sigma^2 + 9\|f\|_\infty) \end{aligned} \quad (8)$$

Based on the result of Lemma 2, we get

$$\begin{aligned} \mathbb{E} \left[(\bar{f}_n(\mathbf{x}) - \hat{f}_n(\mathbf{x}))^2 \right] \\ \leq \frac{(1 + \tau_n)^d e^{d(d-1)} + 1}{n} (2\sigma^2 + 9\|f\|_\infty) \end{aligned} \quad (9)$$

Combining the result of Eq. (6)(9), we get:

$$\begin{aligned} R(\hat{f}_n) \\ \leq \frac{4dL^2}{\tau_n^2} + \frac{(1 + \tau_n)^d e^{d(d-1)} + 1}{n} (2\sigma^2 + 9\|f\|_\infty) \end{aligned} \quad (10)$$

Taking $\tau_n = n^{\frac{1}{d+2}}$ can make $R(\hat{f}_n)$ scales to $\mathcal{O}(n^{-\frac{2}{d+2}})$.

F Additional Experimental Results

Figure 8 illustrates the observed and predicted labels (and their difference) for the UK Apartment Price Data. The online BSP-Forest appears to be able to capture the price variation reasonably well, and provide an accurate prediction of the true test data. Spatially, the prediction error looks broadly pattern free (in colour distribution), indicating that the regression model is adequate for these data.